Simultaneous reconstruction of multiple signaling pathways *via* the prize-collecting Steiner forest problem

Nurcan Tuncbag[1], Alfredo Braunstein[2,3], Andrea Pagnani[3], Shao-Shan Carol Huang[1], Jennifer Chayes[4], Christian Borgs[4], Riccardo Zecchina[2,3], Ernest Fraenkel[1,*]

[1]Department of Biological Engineering, Massachusetts Institute of Technology, Cambridge, MA 02139, USA.

{ntuncbag, shhuang, fraenkel-admin}@mit.edu

[2]Department of Applied Science, Politecnico di Torino, C.so Duca degli Abruzzi 24, 10129 Torino, Italy

{alfredo.braunstein, riccardo.zecchina}@polito.it

[3]Human Genetics Foundation, Via Nizza 52, 10126 Torino, Italy

andrea.pagnani@hugef-torino.org

[4]Microsoft Research New England, One Memorial Drive, Cambridge, MA 02142, USA

{jchayes, borgs}@microsoft.com

*Corresponding author

ABSTRACT

Signaling and regulatory networks are essential for cells to control processes such as growth, differentiation and response to stimuli. Although many "omic" data sources are available to probe signaling pathways, these data are typically sparse and noisy. Thus, it has been difficult to use these data to discover the cause of the diseases and to propose new therapeutic strategies. We overcome these problems and use "omic" data to reconstruct simultaneously multiple pathways that are altered in a particular condition by solving the prize-collecting Steiner forest problem. To evaluate this approach, we use the well-characterized yeast pheromone response. We then apply the method to human glioblastoma data, searching for a forest of trees each of which is rooted in a different cell surface receptor. This approach discovers both overlapping and independent signaling pathways that are enriched in functionally and clinically relevant proteins, which could provide the basis for new therapeutic strategies. Although the algorithm was not provided with any information about the phosphorylation status of receptors, it identifies a small set of clinically relevant receptors among hundreds present in the interactome.

Keywords: prize-collecting Steiner forest, signaling pathways, multiple network reconstruction

1. INTRODUCTION

High-throughput technologies including mass spectrometry, chromatin immunoprecipitation followed by sequencing (CHIP-Seq), RNA sequencing (RNA-seq), microarray and screening methods have the potential to provide dramatically new insights into biological processes. By providing a relatively comprehensive view of the changes that occur for a specific type of molecule or perturbation, these approaches can uncover previously unrecognized processes in a system of interest. However, interpreting these data types together to provide a coherent view of the biological processes is still a challenging task. In order to discover how changes in different classes of molecules relate to each other, it is possible to map the data onto a network of known or predicted interactions. In the ideal case, the observed interactions would all lie near each other in a functionally coherent part of the interaction network (the interactome). However, due to false positives and false negatives in both the "omic" data and the interactome, the true situation is much more complex; advanced algorithms are needed to find meaningful connections among the data. Among the approaches that have been proposed to find these sub-networks from the interactome are network flow optimization (Lan, et al., 2011; Yeger-Lotem, et al., 2009), network propagation (Vanunu, et al., 2010), the Steiner tree approach (Bailly-Bechet, et al., 2010a; Dittrich, et al., 2008; Huang and Fraenkel, 2009), network inference from gene expression (Bailly-Bechet, et al., 2010b; Friedman, 2004), linear programming (Ourfali, et al., 2007), maximum-likelihood (Yeang, et al., 2004), electric circuits (Kim, et al., 2011; Missiuro, et al., 2009; Suthram, et al., 2008), network alignment (Sharan and Ideker, 2006) and Bayesian networks (Akavia, et al., 2010).

In our previous work, we used the prize-collecting Steiner tree formalism to find an optimum tree composed of nodes detected in experiments (terminals) and nodes that were not detected

(Steiner nodes). We assigned costs to each interaction reflecting our confidence that the reported interaction was real and assigned prizes for excluding any of the terminals from the tree based on confidence in the proteomic or transcriptional data. By minimizing the sum of the total cost of all edges in the tree and the total prize of all nodes not contained in the tree, we were able to obtain compact and biologically relevant networks (Bailly-Bechet, et. al., 2010a; Huang and Fraenkel, 2009). Despite the power of Steiner tree approach for identifying functionally coherent networks, it is restricted to discovering a connected subgraph, which may be an inadequate representation for many systems. In particular, we often expect there to be many simultaneously acting biological processes in the cell that may not be connected together by interactions in the currently known interactome. These processes may be unconnected either because they may involve essentially independent cell functions, or simply due to our imperfect knowledge of the interactome.

In this work, we formulate a forest (defined as a disjoint union of trees) approach to identify simultaneously acting pathways in biological networks using both proteomic and transcriptional data, We use a generalization of the message-passing algorithm for the Prize-collecting Steiner Tree (PCST) problem (Bailly-Bechet, et. al., 2010a; Bayati, et al., 2008). We first demonstrate the forest approach by using it to integrate proteomic and transcriptional data in the yeast pheromone response, showing that the forest consists of trees enriched in specific and distinct biological processes. As an additional feature, directed edges, which are particularly useful for representing the effects of enzymes and transcriptional regulators on their targets, are also incorporated.

We reasoned that the Steiner forest approach could be utilized in modeling mammalian signaling where there are many more cell-surface receptors and downstream pathways than in

yeast. In principle, the forest approach could uncover multiple, independent components of the biological response. Although the interactome data are much less complete for mammals than for yeast, we show that the same methods are applicable. We built prize-collecting Steiner forests derived from proteomic data from a model of glioblastoma multiforme (GBM) in which each tree was rooted in a different cell surface receptor representing independent signaling pathways and potential points of therapeutic intervention. The solution reveals several known pathways and some unexpected new ones that are altered in the disease and suggests potential therapeutic strategies. The modified algorithm can now be applied to a wide range of complex systems.

2. METHODS

2.1. Datasets

Throughout this work, two different biological networks are used: the yeast interactome and the human interactome. We refer to nodes with prize values greater than zero as terminal nodes.

2.1.1. Yeast Dataset. The yeast interactome contains 34,712 protein-protein and transcription factor to target interactions between 5,957 nodes. The terminal node set contains 106 differentially phosphorylated proteins detected by mass spectrometry (Gruhler, et al., 2005) and 118 differentially expressed genes (Issel-Tarver, et al., 2002) detected by microarray in response to the mating pheromone alpha factor. The node prizes are computed from the fold changes between treated and non-treated conditions. The edge costs are calculated by taking a negative log of the interaction probability. The details are available in (Huang and Fraenkel, 2009). In this study, we modified the transcription factor–DNA interactions to be directed edges. We also added to the interactome a set of directed edges that represent phosphorylation and

dephosphorylation reactions between kinases, phosphatases and their substrates (Breitkreutz, et al., 2010). If these interactions are available in the original interactome, probabilities are retained. If they are not, the probabilities of these interactions are set uniformly to 0.8, based on the distribution of the probabilities in the original interactome. The final interactome contains 35,998 edges between 5,957 nodes. In both cases, the resulting interactomes are comprised of both undirected and directed edges.

2.1.2. Human Dataset. Protein-protein interactions in the STRING database (version 8.3) are used as the data source for the human interactome (Jensen, et al., 2009). Here, the probabilities from experiments and database evidence channels are combined to obtain the final probability of the interactions. Interactions with a combined probability greater than 0.8 are included in the interactome. The receptor molecules are collected from the Human Plasma Membrane Database (Ben-Shlomo, et al., 2003) where 331 receptors are available in the interactome derived from STRING. The phosphoproteomics data in (Huang, et al., 2007) is combined with the interactome in humans for the GBM test case. From this dataset, 72 proteins containing phophorylated tyrosine peptides are present in our human interactome.

2.2. Prize-Collecting Steiner Tree Problem

For a given, directed or undirected network $G(V, E, c(e), p(v))$ of node set V and edge set E, where a $p(v) \geq 0$ assigns a prize to each node $v \in V$ and $c(e) \geq 0$ assigns a cost to each edge e $\in$ E. The aim is to find a tree $T(V_T,E_T)$, by minimizing the objective function:

$$f(T) = \beta \sum_{v \in V_T} p(v) + \sum_{e \in E_T} c(e) \qquad (1)$$

where the first term is β times the sum of the node prizes not included in the tree *T* and the second part is the sum of the edge costs of *T*. Note that

$$\sum_{v \notin V_T} p(v) = -\sum_{v \in V_T} p(v) + const \qquad (2)$$

so that minimizing *f(T)* amounts to collecting the largest set of high prize vertices while minimizing the set of large cost edges in a trade-off tuned by β. As a starting point, we consider the message-passing algorithm for the PCST problem introduced in (Bailly-Bechet, et. al., 2010a). The message-passing algorithm converts the global problem of finding the optimal tree into a set of local problems that can be solved efficiently. These equations are solved iteratively in a computationally efficient way. Here we present a generalization of the message passing algorithm designed to solve the PCST problem on directed networks (*i.e.* where in general c(e{i,j}) might be different from c(e{j,i})). In this variant, the optimization will be done on directed rooted trees, where choice of the root (which will be part of the candidate tree) is an external parameter of the algorithm.

2.3. Prize-Collecting Steiner Forest (PCSF) Problem

A type of PCSF has already been considered in (Chekuri, et al., 2010; Gupta, et al., 2007). In these works penalties are assigned to each pair of nodes either directly connected in the tree (*i.e.* edges belonging to the forest), or completely disconnected (*i.e.* in different forest components). Here we consider a different PCSF construction for a given, directed or undirected network *G(V, E, c(e), p(v))* of node set *V* and edge set *E*, where a $p(v) \geq 0$ assigns a prize to each node $v \in V$ and $c(e) \geq 0$ that assigns a cost to each edge e ∈ F. The aim is to find a forest $F(V_F,E_F)$ that minimizes the objective function:

$$f'(F) = \beta \sum_{v \notin V_F} p(v) + \sum_{e \in E_F} c(e) + \omega \cdot \kappa \qquad (3)$$

where κ is the number of trees in the forest and ω is new tuning parameter explained below. A practical way of minimizing *f'* consists in casting the PCSF into a PCST on a slightly modified graph. The flowchart of this algorithm is illustrated in **Figure S1**. The idea is to introduce an extra root node v_0 into the network connected to each node $v \in V$ by an edge (v, v_0) with cost ω (Bailly-Bechet, et al., 2009). The PCST algorithm is employed on the resulting graph $H(V \cup \{v_0,\}, E \cup Vx\{v_0,\})$ and the solution will be called *T*. We define the forest *F* as *T* with all edges that point to the root removed. It is straightforward to see that the tree *T* is minimal for *f* if and only if the forest *F* is minimal for *f'*. Typically, the algorithm is run for different values of β and ω.

We used the previously published message-passing approach as the underlying implementation for this forest search (Bailly-Bechet, et. al., 2010a), as many of our networks exceeded the capacity of the linear programming approaches. The message-passing approach is computationally fast and robust to the noise in the network as well. Although this algorithm is not guarranteed to find the optimal solution, in practice the networks it discovers are very similar to the exact solution. Introducing the artificial edges allows the algorithm to identify one or more trees that are only connected to the artificial node and not to each other. Although this modification seems algorithmically straightforward, its biological implications are very important. The concept is illustrated in **Figure 1**. In that example, two distinct pathways are connected only through spurious edges. The main difference between the tree formalism and the forest formalism is that the former one that connects as many of the experimental data as it can in a single network. As a result, it will either have to exclude some of the data that relate to distinct biological processes or add spurious edges to force these data to connect to the tree while the

latter one allows the corresponding nodes to be included in distinct trees. However, the forest formalism is able to locate distinct biological processes into different sub-trees through the artificial node. The artifical node and edges give the flexibility of generating several sub-trees without paying any penalty.

2.4. Tuning the parameters

The parameters to be tuned in this problem are ω and β. The number of components of the solution (κ) depends strongly on the parameter ω, but it also depends on the β value: e.g. for $\beta = 0$ the optimal solution is the empty forest for all values of other parameters. For other values of β, while some sub-trees are composed of a single node, some others are composed of large number of nodes in the resulting forest. A forest with many very small trees (a single node each) would be obtained with very small artificial edges cost. The limiting case in the other direction is a single tree resulting from very large artificial edge cost. Therefore, there is a non-trivial interaction between the two parameters (β and ω). In principle, this two dimensional (β, ω) space of parameters should be explored. In this way, we get many possible types of forest: many small trees, many large trees, few small trees, few large trees (see Supplementary text and **Figure S2**). The effect of ω and β intervals highly depends on the distribution of edge costs and node prizes in the targeted interactome, so these parameters will be different for different datasets. For the yeast dataset, ω values are tuned between [0.005, 0.1] and β values are tuned between [1, 20].

2.5. Functional Annotation

For functional enrichment analysis, the BINGO plug-in (Maere, et al., 2005) of Cytoscape (Shannon, et al., 2003) was used. The p-value significance threshold of 0.05 was used, which is corrected for multiple hypothesis testing, and all yeast proteins were used as the background set

for the yeast dataset. For the human dataset, the functional enrichment is performed by using all human proteins as background set. All network visualizations were performed in Cytoscape (Shannon, et. al., 2003).

3. RESULTS

3.1. Practical advantages of the message passing solution for biological networks

Previous work has shown that the message-passing approximation is faster than the branch-and-cut algorithm and typically finds a comparable value for the objective function. This comparison was performed on a benchmark set that is not related to biological data (Bailly-Bechet, et. al., 2010a). Since the message-passing approach only approximates the exact solution found by the branch-and-cut algorithm, we compared the performance of these two algorithms on phosphoproteomic and transcriptional data from the yeast pheromone response.

We performed an initial analysis to determine the appropriate paramater settings. In the branch-and-cut algorithm the size of the network is controlled only by the beta parameter. In the message-passing algorithm, there is a second parameter, called depth, that can also be used to control the size of the resulting tree. Depth (D) represents the maximum allowed distance between the farthest node in the tree and the root node. Based on these observations, we tested several depth values on the yeast interactome and found depth value equal to 20 produces the best objective function value in the PCST runs on yeast dataset (see **Figure S3a**). To check the robustness of the message-passing algorithm we added noise to edge-weights and re-ran it (see **Figure S3b**). We refer to the solutions of these noisy inputs as suboptimal solutions. The overlap between sub-optimal solutions and the original solution is still very high up to a noise value; therefore, the solution is robust to noise on the yeast pheromone data.

Having identified a suitable range for the parameters, we compared the message-passing algorithm to the branch-and-cut algorithm on the original undirected yeast interactome. As mentioned previously, message-passing algorithm finds a solution to the PCST problem in a computationally very effective way. For example, the branch-and-cut algorithm (Ljubic, et al., 2006) takes 931 seconds to reach the exact solution with an objective value of 2.2123 while message-passing algorithm reports the a solution in 237 seconds with an objective value 2.2178. Critically, we find that the overlap of the nodes between these two solutions is 98.5%. This result shows that almost the same solution is obtained by both algorithms, but the message-passing approach is almost four times faster than the branch-and-cut approach (see **Table S1**). The difference in speed becomes critical when exploring the space of parameters or testing the robustness of solutions.

To analyze the effect of the directionality in the solution, we added directed edges from enzymes to their substrates using the kinase and phophatase interaction network in [16]. The algorithm is able to find a smaller network that still includes the same number of terminals as when only the transcription factor-DNA edges were directed. In these two examples, having more directed edges in the starting interactome results in more compact PCST solutions that connect the same number of protein terminals using fewer intermediate nodes (see **Table S1**). These more compact trees are likely to be more useful for generating testable biological hypothesis, since the Steiner nodes that they include are the ones that are most constrained by the experimentally derived terminals. Further, by adding directions between transcription factors to targets and enzyme to substrate interactions, we are able to obtain condition-specific transcription factors and compact networks.

3.2. The PCSF approach reveals parallel working pathways in addition to hidden individual proteins or genes in yeast pheromone response.

High-throughput experimental methods like mass-spectrometry are capable of simultaneously detecting changes in many distinct biological processes that will not be connected by physical interactions. However, the PCST approach searches for a tree structure in the interactome that connects as many of the experimental data as it can. As a result, it will either have to exclude some of the data that relate to distinct biological process or add spurious edges to force these data to connect to the tree. The main advantage of PCSF approach over PCST is that PCSF does not force the system to be connected in a single network, and it can automatically separate multiple pathways.

We tested the PCSF algorithm using data from the yeast pheromone response, which we had previously analyzed using the prize-collecting Steiner tree approach. The data consist of phosphoproteomic and transcriptional changes induced by mating pheromone, and the network is enriched with directed transcription factor-target and kinase/phosphatase-substrate reactions. The edge costs of the interactome were computed as the negative log of the interaction probabilities, and node prizes were obtained from the scheme detailed in (Huang and Fraenkel, 2009). To explore the space of solutions, we tuned the ω and β parameters between [0.005, 0.1] and [1, 20], respectively. The minimum, maximum and average size and number of trees in the constructed PCSFs are extracted for each (ω, β) pair and the distribution of these values along ω parameter is plotted. We looked for a solution in a region where the number of trees and average size of the trees in the forest are closest to each other. By these criteria, the best solution is found when ω = 0.025 and β = 13 (see **Figure S4**). We note that in order to explore these parameters, we constructed 400 solutions to the PCST problem. This number of calculations is only practical

using the message-passing algorithm, but not with the integer linear programming based approaches.

The solution to PCSF problem places distinct functional classes in seperate sub-trees. In this solution, there are six trees, each containing more than 10 nodes. In **Figure 2,** each tree is labeled with its corresponding pathway. Small sub-trees such as $T_{3\text{-}6}$ are enriched in specific biological processes including the PKC pathway, actin organization, protein folding and kinetochore, and DNA and chromatin pathways, while larger trees contain multiple processes. For example, the largest subtree, T_1, contains the pheromone core MAPK pathway with CDC28 related proteins and the second largest one, T_3, contains transcription and transport processes (see **Figure 2**). There are two different yeast MAPK pathways; the pheromone-induced MAPK and the protein kinase C (PKC) pathways (Buehrer and Errede, 1997; Zarzov, et al., 1996). The PCSF algorithm correctly separates these two pathways into different trees. The largest tree in size is T_1 contains pheromone-induced MAPK pathway but the PKC pathway is located in T_3. While the former one induces cells to differentiate and be prepared for mating, the latter one is involved in cell integrity and new cell wall synthesis.

The core pheromone response pathway component in T_1 includes the STE2 receptor. In this sub-tree, the STE2-GPA1-FUS3 interaction is in the core of pheromone response. In addition, the MAP kinase FUS3 activates several transcription factors such as, STE12, DIG1, DIG2 for the expression of mating related genes. T_1 contains DNA replication proteins and cell cycle proteins associated with CDC28 as well. Here, the connection between the MAP kinase pathway in the pheromone core and the CDC28 associated sub-network is constructed through the interaction between FAR1 and CDC28. FAR1 is a direct inhibitor of CDC28/CLN2 complex and functions in orienting cell polarization. This association blocks the cell cycle progression. FUS3

phosphorylates FAR1, and only phosphorylated FAR1 can associate with CDC28/CLN2 complex. All these interactions and these connected pathways are correctly located into the same sub-tree.

The algorithm correctly identifies SLT2, which was not detected in the phosphoproteomic data, as a key node in regulating new cell wall synthesis. SLT2 is a serine/threonine MAP kinase activated in a cascade starting with PKC. The phosphoproteomic data are not sufficient for the algorithm to pick up the upstream pathway. However, in T_3, the algorithm links SLT2 to several transcription factors that mostly function in cell wall integrity and biosynthesis. SLT2 activates RLM1 (Garcia, et al., 2004), SWI4 (Baetz, et al., 2001) and SWI6 transcription factors. RLM1 functions in the maintenance of cell integrity. SWI4/SWI6 regulates the expression of genes functioning in cell wall synthesis and G1/S transition of the cell cycle.

Transcriptional machinery and transport proteins are located in T_2, seperate from other trees. The connection between transcriptional machinery and cellular transport part is achieved by the interaction between PHO4 and PSE1. Although these two proteins are experimentally undetected, the PCSF algorithm locates them in the same sub-tree. Direct association of PSE1 to PHO4 is required for the import of PHO4 into the nucleus (Kaffman, et al., 1998). Nuclear pore components (NUP60, NUP85, NUP116, NUP159) are located in T_2 because nuclear transport is achieved through the nuclear pore (Kaffman, et. al., 1998). In this sub-tree, the transcription factor PHO2 functions in a combinatorial manner with PHO4 and SWI5 (Bhoite, et al., 2002).

In addition to the pathway analysis, we utilized GO biological process annotations to find the specific biological processes enriched in these trees. In **Table 1**, the top three annotations for each tree are tabulated along with their corrected p-values. These results show that this method effectively locates different biological processes into different trees. Instead of forcing all nodes

to be connected in a single network, this "forest" representation composed of multiple sub-trees is more useful for distinguishing distinct pathways. The forest solution retains more enrichment for the expected biological process, such as response to stress, cell cycle, signaling and transport (see **Figure S5**). Further, by adding directions between transcription factors to targets and enzyme to substrate interactions, we are able to obtain more condition-specific transcription factors and a smaller network that still includes the same number of terminals (see **Table S1** and **SI text**).

To evaluate this approach further, we selected terminals from distinct biological processes assigned by GO annotations and constructed PCSFs. As we show in the supplemental materials, these tests revealed that the approach was able to reconstruct functionally coherent trees based solely on the connectivity of the interactome. The detailed results and the list of biological processes used in this analysis are added to the Supplementary text, **Table S2** and **Figure S6**.

3.3. The PCSF algorithm reveals coordinately acting receptor molecules functioning in human GBM by integrating receptome, interactome and proteomics data.

Having demonstrated that the PCSF algorithm can successfully distinguish parallel-working pathways in yeast, we used it to identify cell surface receptors associated with signaling pathways altered in disease. Cell surface receptors are an interesting class of molecules to study, as they may be particularly easy to target with therapeutic agents. There is increasing evidence that some proteins are "undruggable," in other words hard or impossible to target with small molecule-based therapies because their three-dimensional shape does not have any appropriate concave sites to which these proteins can bind. In contrast, cell surface receptors can either be

targeted with their natural ligand, modified forms of the natural ligand, small molecules that insert into the naturally occurring binding pocket or antibodies.

We modified our approach to identify cell-surface receptors associated with phosphoproteomic changes that occur in a model of glioblastoma (**Figure S7**). We use the artificial node to represent external stimuli (including autocrine loops) that potentially activates multiple receptor molecules, by connecting this node only to cell surface receptors, of which 331 are present in our human interactome. After running the prize-collecting Steiner tree algorithm and removing the artificial node, each sub-tree will contain one receptor as the starting node. The receptors selected in the solution of PCSF represent those most closely connected to the measured phosphoproteomic data and are therefore likely to be main contributors of the disease.

We applied this approach to phosphotyrosine data for a model of human GBM (Huang, et. al., 2007) representing phosphorylation differences between cells expressing an oncogenic mutation in the EGFR protein and cells with an inactive form of this receptor tyrosine kinase. The result is a set of eleven compact trees each rooted in one of the 331 potential receptors. The selected receptors in order of their tree sizes are EGFR, ERBB2, CD36, IGF1R, PTCH1, A2MR, SDC2, MET, ITGB3, NPR1 and EPHA2 (see **Figure 3**). Although the algorithm had no direct knowledge that the data represented the results of mutation in EGFR, it selected this as the root of the largest tree. In fact, each of the four top receptors has a known link to cancer. EGFR and ERBB2 are EGF-family receptors, and it is known that EGFR is mutated in more than 50% GBM cases (Cancer_Genome_Atlas_Research_Network, 2008). IGF1R is overexpressed in many tumors and mediates proliferation and resistance to apoptosis, and it is currently an anti-cancer treatment target (Macaulay, 2004). Because IGF1R is also abnormally active in GBM, its inhibition is presented as a potential therapy to arrest the tumor growth (Kiaris, et al., 2000). It

has been previously shown that the EGF and IGF pathways cross-talk (Adams, et al., 2004), and IGF1R mediates resistance to anti-EGFR therapy in glioma cells (Chakravarti, et al., 2002). Although CD36 functions in brain specific angiogenic regulation (Kaur, et al., 2009) and the interactions between CD36-Fyn-Yes lead to calcium and neurotransmitter release (Silverstein and Febbraio, 2009), its relation to GBM has not been studied in detail. Further, the downstream interactions in Fyn points out the glutamate related proteins GRIN2B and DLG3. In addition to those receptors pictured in **Figure 3**, we identified PTCH1 as an important receptor in glioblastoma which is the root of a small sub-tree. PTCH1 is a known tumor suppressor (Agren, et al., 2004). These less studied receptors, CD36 and PTCH1, suggest novel therapeutic targets for glioblastoma treatment.

Although the algorithm is constrained to identify independent trees, we can observe the potential for cross-talk between different receptors by adding back all the edges among the selected nodes (see **Figure S8**). We noticed two receptors selected by the algorithm, namely MET and ITGB3 (integrin-β3), are also very important, despite the fact that their corresponding sub-trees each contain only two nodes. When all edges are put back in the Steiner forest we observe extensive links between these two receptors and the EGFR sub-tree. MET has links to seven proteins out of nine first neighbors of EGFR and to 16 proteins in total of the EGFR rooted sub-tree, and ITGB3 has links to seventeen members of the EGFR sub-tree. By contrast, IGF1R has links only to three proteins and ERBB2 has link only to two proteins in the first neighbors of EGFR. Although this information was not provided to the algorithm, MET is detected as differentially phosphorylated in the original data, and a MET inhibitor synergizes with an EGFR inhibitor (Huang, et. al., 2007).

Mammalian signaling systems frequently demonstrate a high degree of cross-talk. If two receptors share many common downstream components, the algorithm need only choose one of these as a root node to explain all the terminal nodes. We, therefore, introduce a perturbation-based approach to improve the sensitivity of the algorithm in identifying receptors that share many downstream components with the selected root nodes. In this analysis, selected receptor molecules (the root of the largest tree in the forest and other receptors in its corresponding sub-family available in the forest) and all their interactions are removed from the interactome and PCSF algorithm is applied to the remaining network. Through this *in silico* knock-out experiment, we can find the other receptor molecules whose role may be masked in the presence of the receptors in the initial forest.

We first knocked-out two EGF/ERBB sub-family receptors, EGFR and ERBB2, from the network and re-generated the PCSF. In the resulting network, 37 out of 42 nodes in the down-stream of EGFR in the original tree are connected to other receptors. PDGFR (Platelet-derived growth factor receptor) is the root of the largest tree, covering 23 nodes linked to EGFR in the original network (shown in **Figure S9a**). This observation suggests that PDGFR may have many overlapping functions with EGFR. In fact, several studies have shown that PDGFR is critical in brain tumorogenesis (Dai, et al., 2001; Uhrbom, et al., 1998); mutation of PDGFR causes alteration in the intracellular signaling (Clarke and Dirks, 2003) and it is a therapeutic target in GBM (Ziegler, et al., 2008). Another 14 nodes down-stream of EGFR are shared by MET (seven nodes), IGF1R (five nodes) and ITGB3 (two nodes). Although these four receptors (PDGFR, MET, IGF1R and ITGB3) capture many of the nodes that were down-stream of EGFR, five nodes are not captured by any other receptors. These may represent signaling that is uniquely downstream of EGFR.

To further explore the network, we removed PDGFR in addition to EGFR and ERBB2. In the new network, the MET receptor partially replaces PDGFR. It has been shown that the MET receptor is activated in GBM and it might be a therapeutic target (Li, et al., 2011). Similar to the MET receptor tree, the sub-tree containing ITGB3 receptor also collects several of the nodes previously associated with EGFR in its corresponding sub-tree (shown in **Figure S9b**). It is interesting to note that integrins function as both upstream and downstream effectors of growth factor receptors, such as EGFR, IGF1R, PDGFR, MET (Alam, et al., 2007). Integrins and their relation to GBM have not been studied in detail, which may have clinical importance in GBM.

During all these leave-one-receptor-out tests, IGF1R is present in the resulting PCSF, and it retains all proteins in the original network. The downstream network of IGF1R starts with the estrogen receptor (ESR1) interaction and it contains several MAPKs. It has been shown that ESR1 and IGF1R are cross-regulated in the brain and activate the MAPK/ERK pathway. This system of interactions results in some neural functional regulations in the brain; such as, synaptic plasticity, neurotic growth, and neuronal survival (Cardona-Gomez, et al., 2002). The size of the trees corresponding to the down-stream of MET and ITGB3 receptors increases at each knock-out. Also, the FYN related downstream pathway of CD36 is swapped to be downstream of MET receptor, although CD36 is not knocked-out. This result implies that FYN-related pathway may be activated by several receptors.

To further validate the relevancy of these receptor molecules (EGFR, ERBB2, IGF1R, CD36, PDGFR, MET and ITGB3), we used the TCGA GBM Gene Ranker (http://cbio.mskcc.org/tcga-generanker/). This server combines available literature information and TCGA data for individual genes to score them. All selected receptors are among highly ranked genes (genes having a score greater than 2.0) in GBM (calculated scores are as follows: EGFR: 15.75, MET:

11.75, ERBB2: 9.25, PDGFRB: 7.25, IGF1R: 4.0, ITGB3: 3.75, CD36: 2.0), with EGFR, MET and ERBB2 having the highest rank in the database.

We performed randomization tests to check the reliability of the output of the algorithm. Here, terminal nodes, their prizes and the parameter set are kept same with the original PCSF analysis of GBM. In addition, number of nodes, edges and edge costs are the same as in the original interactome. Only the edges are re-shuffled randomly within the network. The randomization test is repeated ten times on different interactomes. The statistics for the average of the resulting forests are tabulated in **Table S3**.These characteristics show that random PCSFs contain many more sub-trees when compared to the original PCSF and these sub-trees are not structured like the original trees; most of the trees in the random forests are 'stringy', composed of nine proteins at most. Further, random trees are not enriched for a specific biological process and none of the receptors found in the original PCSF are selected in the random PCSFs. The algorithm uses substantially more Steiner nodes to connect terminal nodes in random case. We performed another randomization test by reshuffling the nodes in the original interactome. In this way, the degree distribution is retained. In these randomizations we retain the same terminal nodes, prizes and the parameter set are kept same with the original PCSF analysis, but these proteins have now been randomly mapped to other nodes. The results show that the characteristics of the sub-trees in the random PCSFs are similar with the previous random case; they are 'stringy', not structured and not enriched for functions. However, this time the total number of nodes included in the PCSF is not as large as in the previous random case. These results show that the real PCSF solution is significantly different than the random solutions. It is particularly important that the receptors found by the algorithm run on the GBM data are not

selected in the randomizations, supporting the hypothesis that these receptors are biologically relevant.

4. DISCUSSION

We present a method for simultaneously discovery of multiple pathways by searching for "forests" consisting of multiple trees. We are able to solve this problem efficiently, even for large human networks by a simple modification of the previously published message-passing solution for the Steiner tree problem. When applied to the pheromone response data on the directed yeast interactome, the PCSF approach reveals several parallel pathways affected by yeast pheromone. Some of these parallel pathways contain multiple, coherently acting processes, such as pheromone response and the CDC28 associated pathway, or transport and transcriptional activity of PHO4. Others contain only one process, such as actin organization or protein folding. Independently from the pheromone response network, we also show that this approach can identify regions of the yeast interactome enriched in various biological processes using only the connectivity information (Supplementary Information).

The advantages of the forest approach are most apparent when used to study mammalian cells, which respond to a large number of hormones, growth factors and cytokines. Applying this approach to proteomic data from a model of GBM results in a forest composed of several sub-trees, each of which is rooted from a receptor molecule. The PCSF algorithm is able to select receptors relevant to GBM from hundreds of molecules in the human receptome. The solution reveals several known pathways and some unexpected new ones. EGFR, ERBB2, IGF1R and CD36 are starting nodes of the largest sub-trees in the PCSF. This set of receptor molecules was selected by the algorithm among hundreds of receptors, and the literature search shows that each of the selected receptors is clinically relevant to GBM.

To find additional receptors whose downstream signaling pathways overlap with the selected receptors, we used an iterative approach that can be thought of as an *in silico* knock-out experiment. In this analysis, a selected receptor molecule and all its interactions are removed from the interactome and PCSF algorithm is applied to the remaining network. These calculations revealed the roles of PDGFR, MET and ITGB3 all of which have been previously linked to GBM.

Our method can be efficienly utilized to reconstruct networks that are enriched in functionally and clinically relevant proteins. Further, the algorithm is flexible, and can be modified for other types of data such as protein-small molecule inhibitor interactions and protein-metabolite interactions.

Acknowledgements. We thank Dr. Sara Gosline from MIT and Dr. Oznur Tastan from Microsoft Research for their critical reading and fruitful comments. This work is supported by NIH grants U54CA112967 and R01GM089903 and used computing resources funded by the National Science Foundation under Award No. DB1-0821391. EF receives support from the Eugene Bell Career Development Chair. RZ acknowledges the ERC grant OPTINF 267915. The support from the EC grant STAMINA 265496 is also acknowledged by AB and RZ.

REFERENCES

Adams T.E., McKern N.M., Ward C.W. 2004. Signalling by the type 1 insulin-like growth factor receptor: interplay with the epidermal growth factor receptor. *Growth Factors* 22, 89-95.

Agren M., Kogerman P., Kleman M.I., et al. 2004. Expression of the PTCH1 tumor suppressor gene is regulated by alternative promoters and a single functional Gli-binding site. *Gene* 330, 101-14.

Akavia U.D., Litvin O., Kim J., et al. 2010. An integrated approach to uncover drivers of cancer. *Cell* 143, 1005-17.

Alam N., Goel H.L., Zarif M.J., et al. 2007. The integrin-growth factor receptor duet. *J Cell Physiol* 213, 649-53.

Baetz K., Moffat J., Haynes J., et al. 2001. Transcriptional coregulation by the cell integrity mitogen-activated protein kinase Slt2 and the cell cycle regulator Swi4. *Mol Cell Biol* 21, 6515-28.

Bailly-Bechet M., Borgs C., Braunstein A., et al. 2010a. Finding undetected protein associations in cell signaling by belief propagation. *Proc Natl Acad Sci U S A* 108, 882-7.

Bailly-Bechet M., Bradde S., Braunstein A., et al. 2009. Clustering with shallow trees. *J.Stat.Mech.* P12010.

Bailly-Bechet M., Braunstein A., Pagnani A., et al. 2010b. Inference of sparse combinatorial-control networks from gene-expression data: a message passing approach. *BMC Bioinformatics* 11, 355.

Bayati M., Borgs C., Braunstein A., et al. 2008. Statistical mechanics of steiner trees. *Phys Rev Lett* 101, 037208.

Ben-Shlomo I., Yu Hsu S., Rauch R., et al. 2003. Signaling receptome: a genomic and evolutionary perspective of plasma membrane receptors involved in signal transduction. *Sci STKE* 2003, RE9.

Bhoite L.T., Allen J.M., Garcia E., et al. 2002. Mutations in the pho2 (bas2) transcription factor that differentially affect activation with its partner proteins bas1, pho4, and swi5. *J Biol Chem* 277, 37612-8.

Breitkreutz A., Choi H., Sharom J.R., et al. 2010. A global protein kinase and phosphatase interaction network in yeast. *Science* 328, 1043-6.

Buehrer B.M., Errede B. 1997. Coordination of the mating and cell integrity mitogen-activated protein kinase pathways in Saccharomyces cerevisiae. *Mol Cell Biol* 17, 6517-25.

Cancer_Genome_Atlas_Research_Network. 2008. Comprehensive genomic characterization defines human glioblastoma genes and core pathways. *Nature* 455, 1061-8.

Cardona-Gomez G.P., Mendez P., DonCarlos L.L., et al. 2002. Interactions of estrogen and insulin-like growth factor-I in the brain: molecular mechanisms and functional implications. *J Steroid Biochem Mol Biol* 83, 211-7.

Chakravarti A., Loeffler J.S., Dyson N.J. 2002. Insulin-like growth factor receptor I mediates resistance to anti-epidermal growth factor receptor therapy in primary human glioblastoma cells through continued activation of phosphoinositide 3-kinase signaling. *Cancer Res* 62, 200-7.

Chekuri C., Ene A., Korula N. 2010. Prize-Collecting Steiner Tree and Forest in Planar Graphs. *Data Structures and Algorithms*.

Clarke I.D., Dirks P.B. 2003. A human brain tumor-derived PDGFR-alpha deletion mutant is transforming. *Oncogene* 22, 722-33.

Dai C., Celestino J.C., Okada Y., et al. 2001. PDGF autocrine stimulation dedifferentiates cultured astrocytes and induces oligodendrogliomas and oligoastrocytomas from neural progenitors and astrocytes in vivo. *Genes Dev* 15, 1913-25.

Dittrich M.T., Klau G.W., Rosenwald A., et al. 2008. Identifying functional modules in protein-protein interaction networks: an integrated exact approach. *Bioinformatics* 24, i223-31.

Friedman N. 2004. Inferring cellular networks using probabilistic graphical models. *Science* 303, 799-805.

Garcia R., Bermejo C., Grau C., et al. 2004. The global transcriptional response to transient cell wall damage in Saccharomyces cerevisiae and its regulation by the cell integrity signaling pathway. *J Biol Chem* 279, 15183-95.

Gruhler A., Olsen J.V., Mohammed S., et al. 2005. Quantitative phosphoproteomics applied to the yeast pheromone signaling pathway. *Mol Cell Proteomics* 4, 310-27.

Gupta A., Konemann J., Leonardi S., et al. 2007. An efficient cost-sharing mechanism for the prize-collecting Steiner forest problem. *SODA '07 Proceedings of the eighteenth annual ACM-SIAM symposium on Discrete algorithms*.

Huang P.H., Mukasa A., Bonavia R., et al. 2007. Quantitative analysis of EGFRvIII cellular signaling networks reveals a combinatorial therapeutic strategy for glioblastoma. *Proc Natl Acad Sci U S A* 104, 12867-72.

Huang S.S., Fraenkel E. 2009. Integrating proteomic, transcriptional, and interactome data reveals hidden components of signaling and regulatory networks. *Sci Signal* 2, ra40.

Issel-Tarver L., Christie K.R., Dolinski K., et al. 2002. Saccharomyces Genome Database. *Methods Enzymol* 350, 329-46.

Jensen L.J., Kuhn M., Stark M., et al. 2009. STRING 8--a global view on proteins and their functional interactions in 630 organisms. *Nucleic Acids Res* 37, D412-6.

Kaffman A., Rank N.M., O'Shea E.K. 1998. Phosphorylation regulates association of the transcription factor Pho4 with its import receptor Pse1/Kap121. *Genes Dev* 12, 2673-83.

Kaur B., Cork S.M., Sandberg E.M., et al. 2009. Vasculostatin inhibits intracranial glioma growth and negatively regulates in vivo angiogenesis through a CD36-dependent mechanism. *Cancer Res* 69, 1212-20.

Kiaris H., Schally A.V., Varga J.L. 2000. Antagonists of growth hormone-releasing hormone inhibit the growth of U-87MG human glioblastoma in nude mice. *Neoplasia* 2, 242-50.

Kim Y.A., Wuchty S., Przytycka T.M. 2011. Identifying causal genes and dysregulated pathways in complex diseases. *PLoS Comput Biol* 7, e1001095.

Lan A., Smoly I.Y., Rapaport G., et al. 2011. ResponseNet: revealing signaling and regulatory networks linking genetic and transcriptomic screening data. *Nucleic Acids Res.*

Li Y., Li A., Glas M., et al. 2011. c-Met signaling induces a reprogramming network and supports the glioblastoma stem-like phenotype. *Proc Natl Acad Sci U S A* 108, 9951-6.

Ljubic I., Weiskircher R., Pferschy U., et al. 2006. An algorithmic framework for the exact solution of the Prize-Collecting Steiner Tree Problem. *Mathematical Programming* 105, 427-449.

Macaulay V.M. 2004. The IGF receptor as anticancer treatment target. *Novartis Found Symp* 262, 235-43; discussion 243-6, 265-8.

Maere S., Heymans K., Kuiper M. 2005. BiNGO: a Cytoscape plugin to assess overrepresentation of gene ontology categories in biological networks. *Bioinformatics* 21, 3448-9.

Missiuro P.V., Liu K., Zou L., et al. 2009. Information flow analysis of interactome networks. *PLoS Comput Biol* 5, e1000350.

Ourfali O., Shlomi T., Ideker T., et al. 2007. SPINE: a framework for signaling-regulatory pathway inference from cause-effect experiments. *Bioinformatics* 23, i359-66.

Shannon P., Markiel A., Ozier O., et al. 2003. Cytoscape: a software environment for integrated models of biomolecular interaction networks. *Genome Res* 13, 2498-504.

Sharan R., Ideker T. 2006. Modeling cellular machinery through biological network comparison. *Nat Biotechnol* 24, 427-33.

Silverstein R.L., Febbraio M. 2009. CD36, a scavenger receptor involved in immunity, metabolism, angiogenesis, and behavior. *Sci Signal* 2, re3.

Suthram S., Beyer A., Karp R.M., et al. 2008. eQED: an efficient method for interpreting eQTL associations using protein networks. *Mol Syst Biol* 4, 162.

Uhrbom L., Hesselager G., Nister M., et al. 1998. Induction of brain tumors in mice using a recombinant platelet-derived growth factor B-chain retrovirus. *Cancer Res* 58, 5275-9.

Vanunu O., Magger O., Ruppin E., et al. 2010. Associating genes and protein complexes with disease via network propagation. *PLoS Comput Biol* 6, e1000641.

Yeang C.H., Ideker T., Jaakkola T. 2004. Physical network models. *J Comput Biol* 11, 243-62.

Yeger-Lotem E., Riva L., Su L.J., et al. 2009. Bridging high-throughput genetic and transcriptional data reveals cellular responses to alpha-synuclein toxicity. *Nat Genet* 41, 316-23.

Zarzov P., Mazzoni C., Mann C. 1996. The SLT2(MPK1) MAP kinase is activated during periods of polarized cell growth in yeast. *Embo J* 15, 83-91.

Ziegler D.S., Wright R.D., Kesari S., et al. 2008. Resistance of human glioblastoma multiforme cells to growth factor inhibitors is overcome by blockade of inhibitor of apoptosis proteins. *J Clin Invest* 118, 3109-22.

TABLES

Table 1 GO enrichments of the sub-trees in the PCSF illustrated in **Fig.2**.

Subtree Name	**GO Enrichment - Biological Process**	**Corr p-value**
T_1	regulation of cell cycle	1.97×10^{-17}
	cell division	2.60×10^{-17}
	cell cycle	3.02×10^{-17}
T_2	transcription	7.07×10^{-13}
	regulation of nucleobase, nucleoside, nucleotide and nucleic acid metabolic process	2.36×10^{-12}
	nuclear transport	7.30×10^{-8}
T_3	positive regulation of gene-specific transcription	2.20×10^{-5}
	regulation of gene-specific transcription	7.75×10^{-5}
	positive regulation of transcription, DNA-dependent	9.11×10^{-5}
T_4	actin filament-based process	1.51×10^{-9}
	endocytosis	4.42×10^{-9}
	actin cytoskeleton organization	9.32×10^{-9}
T_5	protein folding	1.60×10^{-3}
	protein refolding	1.60×10^{-3}
	kinetochore assembly	4.25×10^{-3}
T_6	positive regulation of glycolysis	2.54×10^{-4}
	regulation of glycolysis	2.54×10^{-4}
	positive regulation of transcription	2.54×10^{-4}

FIGURES

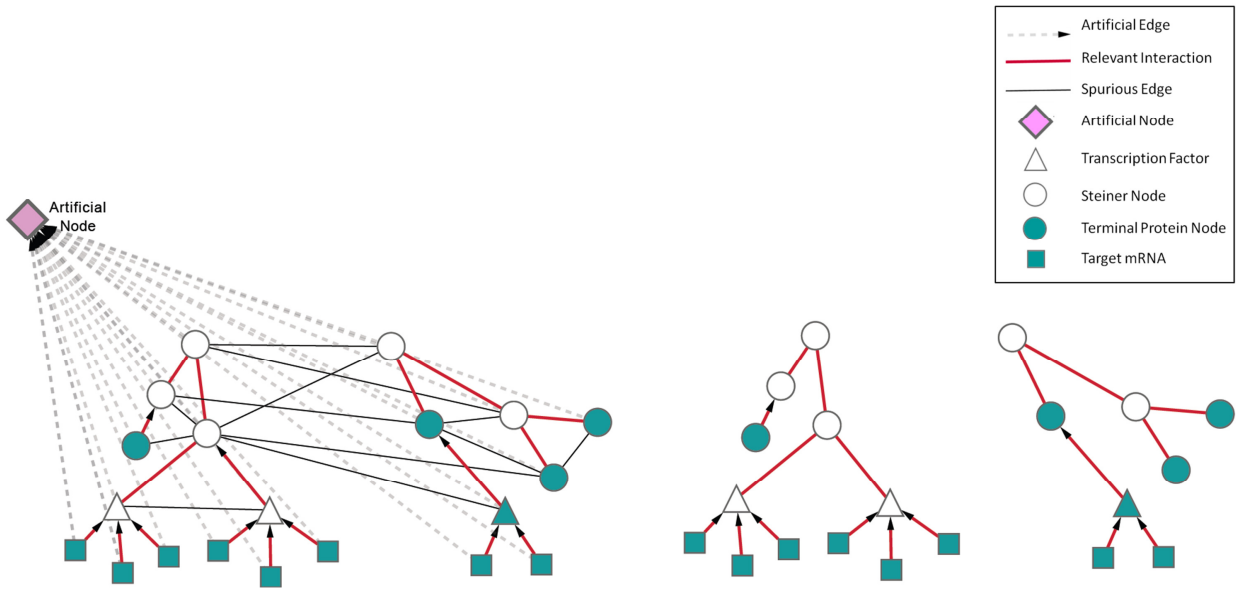

FIG. 1. Conceptual illustration of the PCSF algorithm. The left panel shows an interactome and the right panel shows the Steiner forest constructed from that interactome. The direction of transcription factor to target and kinase/phosphatase to substrate interactions are pointing towards the root node (opposite to the biological direction). In this scenario, there are spurious edges between these two pathways in the interactome. The PCSF algorithm provides the advantage to connect these distinct pathways artificially.

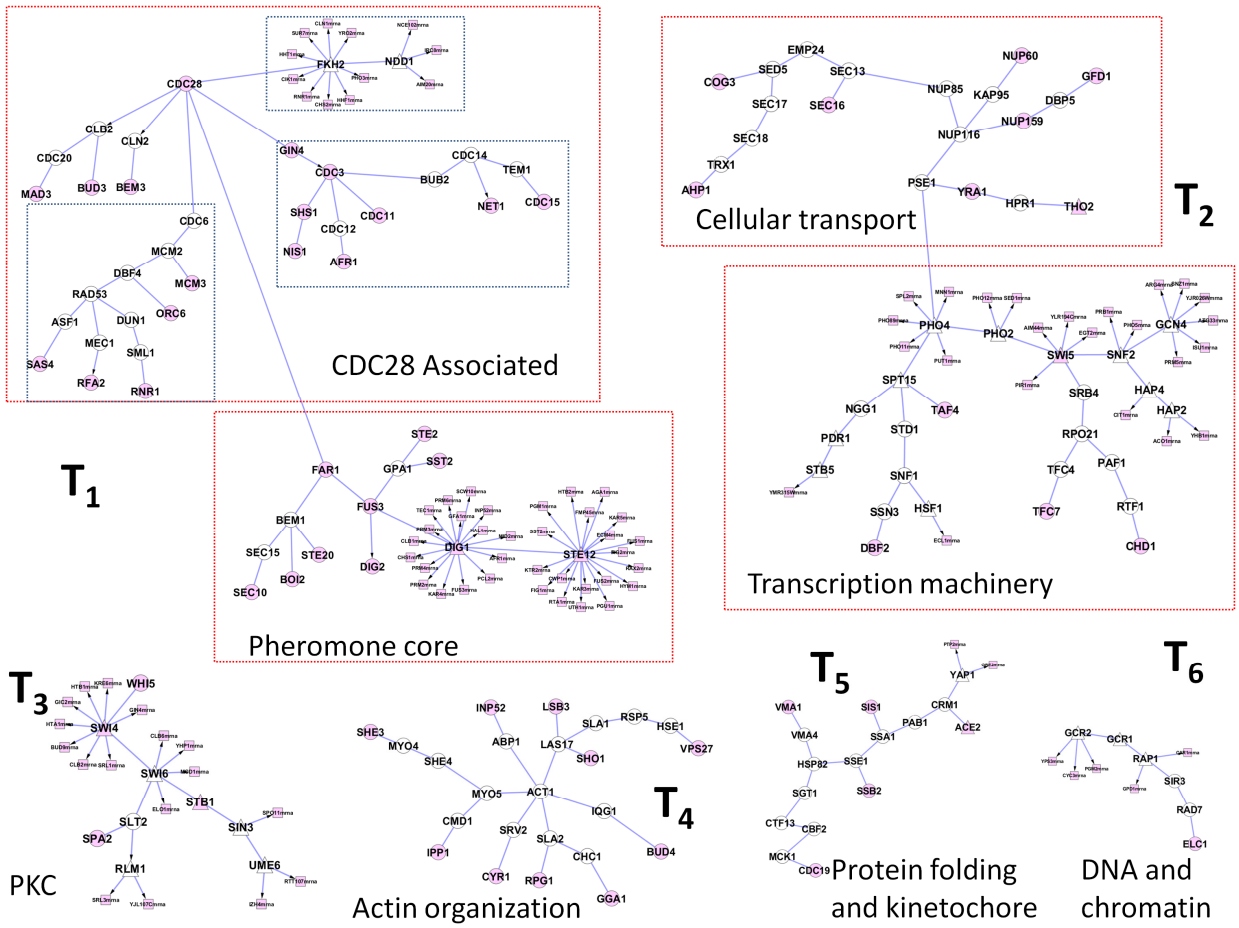

FIG. 2. Prize-collecting Steiner Forest (PCSF) of the Yeast Pheromone Response Network. Functional groups annotated by Gene Ontology (GO) are tagged with red boxes. In this PCSF, the rectangular nodes are DNA, triangular nodes are transcription factors and the circular nodes are proteins. Terminal nodes are colored red.

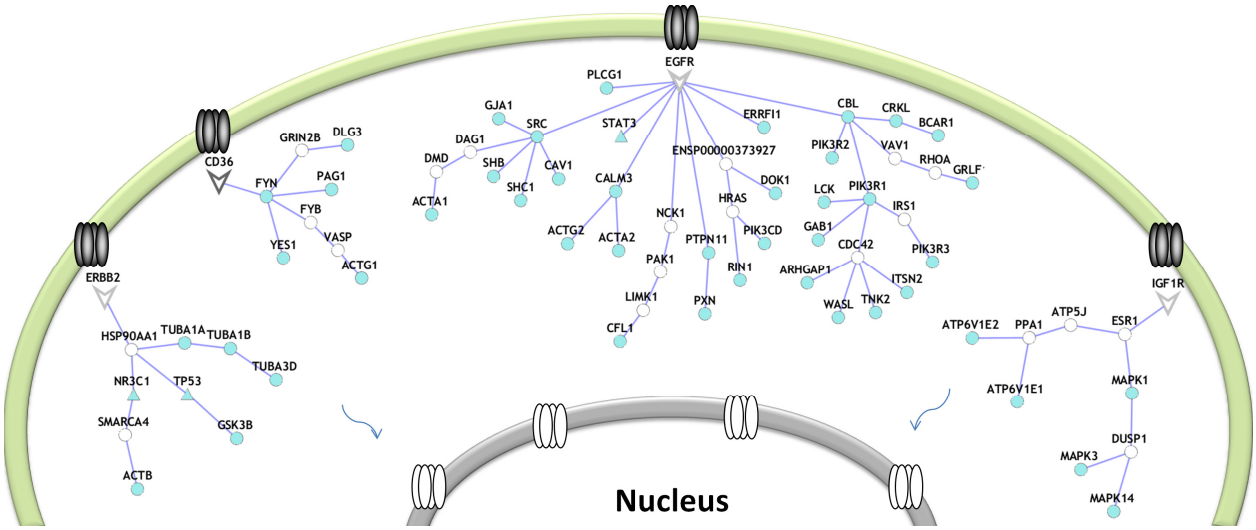

FIG. 3. Network representation of the PCSF for human glioblastoma dataset. Each tree is rooted from a cell surface receptor. The receptor molecules are represented by the arrowheads, transcription factors in triangles and other proteins as circles. Terminal nodes are colored in cyan.

SUPPLEMENTARY INFORMATION

Simultaneous reconstruction of multiple signaling pathways *via* the prize-collecting Steiner forest problem

Nurcan Tuncbag[1], Alfredo Braunstein[2,3,4], Andrea Pagnani[2], Shao-Shan Carol Huang[1], Jennifer Chayes[5], Christian Borgs[5], Riccardo Zecchina[2,3,4], Ernest Fraenkel[1]

Tuning parameters for the prize-collecting Steiner forest problem

The flowchart of PCSF algorithm is illustrated in **Figure S1**. The idea is to introduce an extra root node v_0 into the network connected to each node $v \in V$ by an edge (v, v_0) with cost ω. We first evaluated the effect of the parameters on the forest algorithm by applying it to random networks. We generated two random datasets with very different characteristics. The first one is composed of 3,000 nodes and 7,500 edges with each node has a fixed degree 5. Edge costs and penalties are uniformly distributed over [0, 1]. All nodes have a penalty value. The second dataset is composed of 3,000 nodes and 15,000 edges where each node has a degree of 10. Edge costs follow a bi-modal distribution with modes at 20 and 80. Node penalties follow a tri-modal distribution with modes at 20, 80 and 160 and all of the nodes have a penalty value.

The PCST runs show that the message passing and branch-and-cut algorithms achieve the same objective function value (550 for random set 1, 68,800 for random set 2); however, message-passing approach reaches the optimum solution faster (10 and 168 sec, respectively) than the branch-and-cut algorithm (235 and 1043 sec, respectively). As shown in **Figure S2**, if the edge costs are uniformly distributed, the number and size of the PCSF output are smoothly distributed. However, in the case of bi-modal edge weights, subtrees in the PCSF in size are not uniformly distributed along the changing ω value. For the first random dataset, the ω values are selected between [0.1, 2] and β is calculated from $\beta = \omega * \beta_0$ with β_0 values in the range [1, 20]. In this way, 400 different (β, ω) pairs were generated, from which 400 different artificial networks were constructed. For the second random dataset, the ω values are selected between [10, 200] and the β_0 values are changed in the range [1, 20].

To explore the space of solutions in the yeast pheromone response network, we tuned the ω and β parameters between [0.005, 0.1] and [1, 20], respectively. The minimum, maximum and average size and number of trees in the constructed PCSFs are extracted for each (ω, β) pair. In **Figure S4**, the distribution of these values along ω parameter is shown. We looked for a solution in a region that the number of trees and average size of the trees in the forest are closest to each other. By these criteria, the best solution is found when $\omega = 0.025$ and $\beta = 13$. In **Figure S4**, this region is labeled with a red square. We note that in order to explore these parameters, we constructed 400 solutions to the PCST problem. This number of calculations is only practical using the message-passing algorithm, but not with the ILP-based approach.

When compared to the Steiner tree solution, the Steiner forest contains fewer non-terminal (Steiner) nodes, but the nodes that it retains show more enrichment for the expected biological process. The forest solution contains 86 non-terminal nodes, compared to 107 in the tree. Yet the more compact solution to the forest problem has a higher fraction of non-terminals relating to response to stress, cell cycle, signaling and transport (see **Figure S5**).

The PCSF algorithm is able to distinguish different biological processes on the yeast interactome.

We evaluated the PCSF algorithm by examining whether it could identify networks of functionally related proteins in the yeast interactome. In our first test, we selected 21 proteins annotated to be associated with apoptosis and 34 annotated to the pheromone process response, and we assigned these nodes uniform penalties. Applying the PCSF algorithm results in three sub-trees (see **Fig. S6A**), one of which is dominated by apoptotic termini (T2, seven apoptotic termini), the other by pheromone response (T3, ten pheromone response termini), and the third containing members of each set. Including the Steiner nodes in the analysis, we find that one tree (T1) is mostly composed of proteins involved in response to pheromone (p-value=4.13×10^{-18}), regulation of cell cycle (p-value=5.71×10^{-10}) and signal transduction (p-value=4.97×10^{-10}); another tree (T3) is more enriched in reproduction (p-value=9.11×10^{-13}), cell budding (9.83×10^{-4}), actin cytoskeleton organization (p-value=1.49×10^{-4}) and in response to pheromone (3.43×10^{-17}); T2 is functioning mostly in apoptosis and biogenesis (p-value= 1.93×10^{-9}).

We compared the forest solution to that obtained by running the tree algorithm and then clustering the single tree into subtrees by edge betweenness. The non-terminal nodes in T1 of the PCSF are more significantly enriched in cell cycle when compared to the non-terminal nodes in the corresponding cluster in PCST (see **Fig. S6B**). In T2, the non-terminal nodes are more enriched in transport process when compared to its corresponding cluster in PCST. In T3, there are eight non-terminal nodes and three of them (CDC24, FAR1 and AKR1) function in pheromone-dependent signal transduction involved in conjugation with cellular fusion. Two of these non-terminal nodes (CDC24 and AKR1) are present in the corresponding cluster in PCST.

It is interesting that the algorithm rooted each sub-tree with a Steiner node that turns out to be functionally related to its tree. The proteins connected to the artificial node are CDC14 (in T1), DCP1 (in T2) and BEM1 (in T3). The phenotypes of these three proteins (obtained from Yeast Genome Database (Issel-Tarver, et al., 2002)) are consistent with the enrichments in the sub-trees. When Bem1 is knocked-out, the cell shape becomes abnormal and mating efficiency decreases. When CDC14 is knocked-out, cells are not viable and cell cycle progression is arrested. DCP1 deletion results in decreased apoptosis.

To conduct a more general analysis of the PCSF algorithm, we selected proteins from 17 different biological processes as terminal nodes (see **Table S2** for details). The resulting PCSF consists of 11 sub-trees containing more than 10 nodes each. The enrichment of the biological

processes shows again that the larger subtrees combine multiple processes. For example, the largest sub-tree (178 nodes) in the PCSF is enriched in ubiquitin-dependent protein catabolic process (p-value= 1.59×10^{-41}), signaling and cell cycle (p-value= 1.65×10^{-20}) and its non-terminal nodes are enriched in cell cycle (p-value= 2.45×10^{-11}). The second and third largest sub-trees are enriched only in transcription (p-values are 2.81×10^{-54} and 2.01×10^{-54} respectively). Examples of small sized sub-trees include T7, which is enriched in cell division (p-value= 9.91×10^{-10}) and whose non-terminal nodes are enriched especially in M phase (p-value= 8.59×10^{-12}). T8 is enriched overall in DNA repair (p-value=1.68×10^{-9}) and the non-terminals are enriched in DNA repair and replication (p-value= 5.77×10^{-8}). T9 is enriched in Golgi vesicle transport including and excluding the terminal nodes. Thus, the algorithm is able to identify efficiently functionally coherent subtrees from sparse sets of termini.

Table S1 Comparison of the PCST results on directed and undirected interactomes.

Dataset	**# of Nodes**	**# of Interactions**	**PCST size**	**Included Protein Terminals**	**Included DNA Terminals**	**Time to reach the solution (sec)[a]**	**Best optimum solution value**	**Overlap with the solution in (Huang and Fraenkel, 2009)[b]**
Yeast Dataset (undirected)	5,957	34,712	269	62	100	237	2.2178	98.5%
Yeast Dataset (with directed transcription factor-target interactions)	5,957	34,712	221	62	81	115	1.7967	92.7%
Yeast Dataset (with directed transcription factor-target and kinase/phosphatase-substrate interactions)	5,957	35,998	214	62	80	127	1.7975	94.4 %

[a] the time to reach solution by using message-passing approach.
[b] the overlap is calculated only for the yeast datasets.

Table S2 Biological processes with nodes that are connected to each other by relatively reliable interactome data. For each biological process, we generated a histogram illustrating the distribution of the edge costs. If at least 40% of the edge costs are in the top half of the edge costs in the total interactome and total number of nodes is more than 20, proteins in these biological processes are used as terminal nodes in PCSF analysis.

GO ID	Definition
GO:0006366	transcription from RNA polymerase II promoter
GO:0016573	histone acetylation
GO:0019236	response to pheromone
GO:0006461	protein complex assembly
GO:0016311	dephosphorylation
GO:0030242	peroxisome degradation
GO:0006470	protein dephosphorylation
GO:0045944	positive regulation of transcription from RNA polymerase II promoter
GO:0001403	invasive growth in response to glucose limitation
GO:0006302	double-strand break repair
GO:0000122	negative regulation of transcription from RNA polymerase II promoter
GO:0008361	regulation of cell size
GO:0006511	ubiquitin-dependent protein catabolic process
GO:0070481	nuclear-transcribed mRNA catabolic process, non-stop decay
GO:0045893	positive regulation of transcription, DNA-dependent
GO:0007124	pseudohyphal growth
GO:0006891	intra-Golgi vesicle-mediated transport

Table S3 Characteristics of the PCSFs generated from the original interactome and random interactomes using original terminal set.

	Original Interactome	Random Interactome (Edge-reshuffled case)	Random Interactome (Node-reshuffled case)
Maximum size of the sub-trees	43	9	15
Mean size of the sub-trees	8.2	3.8	4.6
Number of sub-trees	12	47	26
Total number of nodes in PCSF	98	180	112

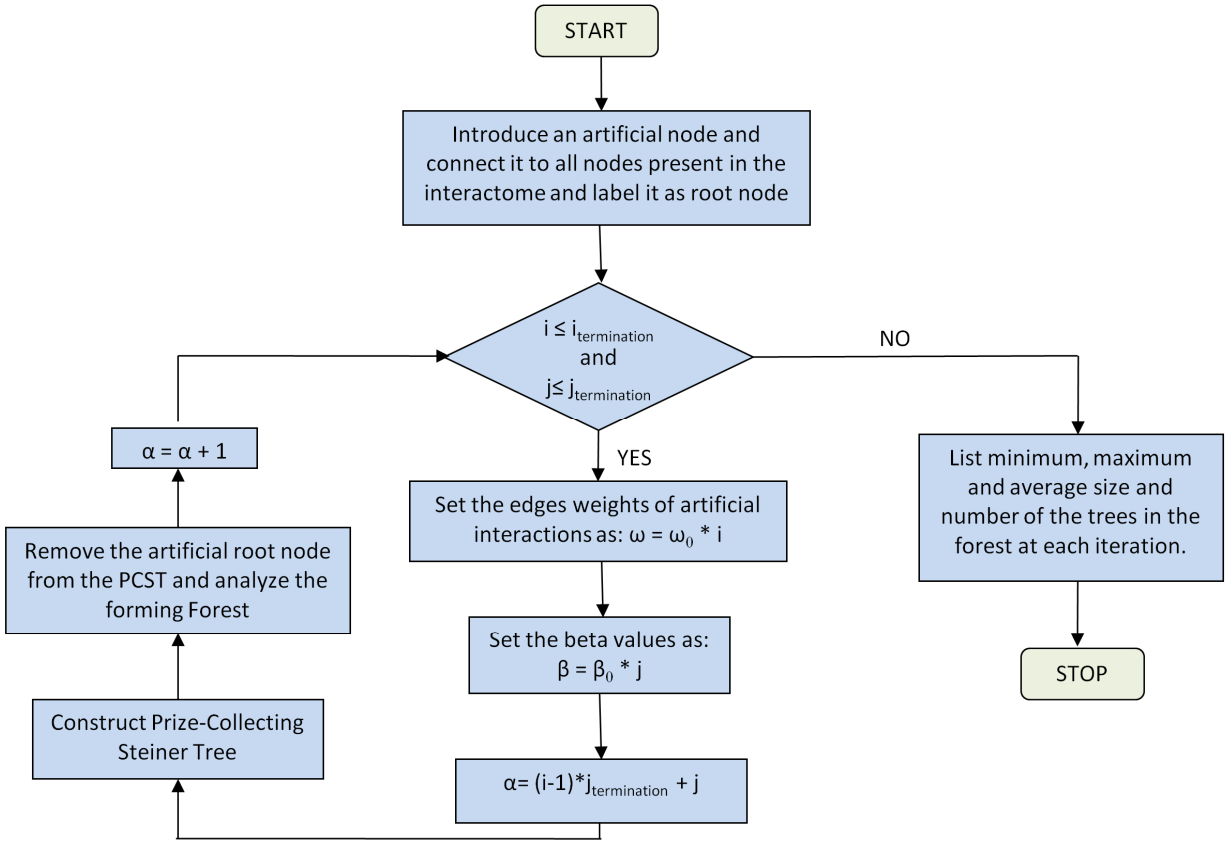

Figure S1 The flowchart of the Prize-Collecting Steiner Forest algorithm. Here, the loop is initialized with i and j each set to 1. We specify that the loop continues while i and j are not equal to $i_{termination}$ and $j_{termination}$, respectively. In the body of the loop, we increment i and j by 1. Also, α counts the iteration steps.

(a)

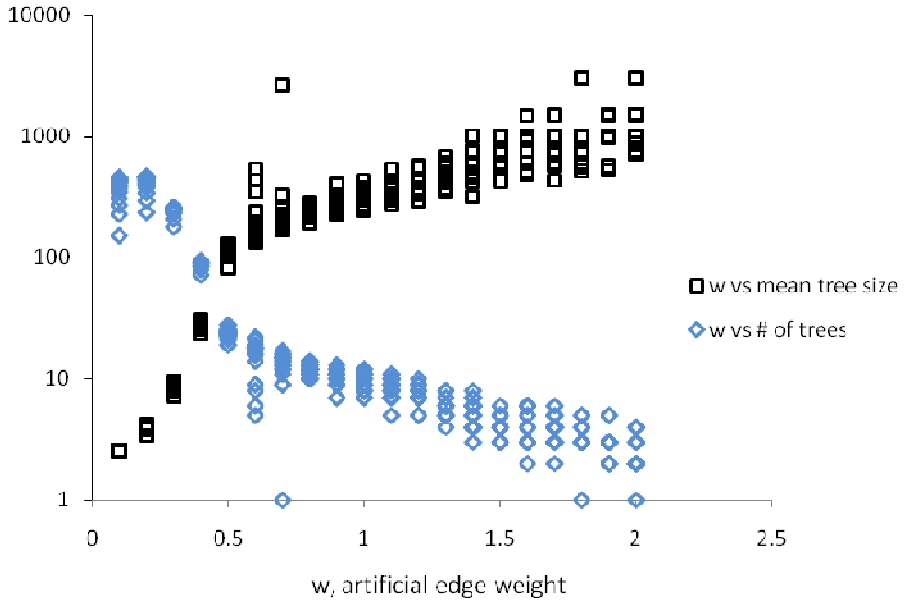

(b)

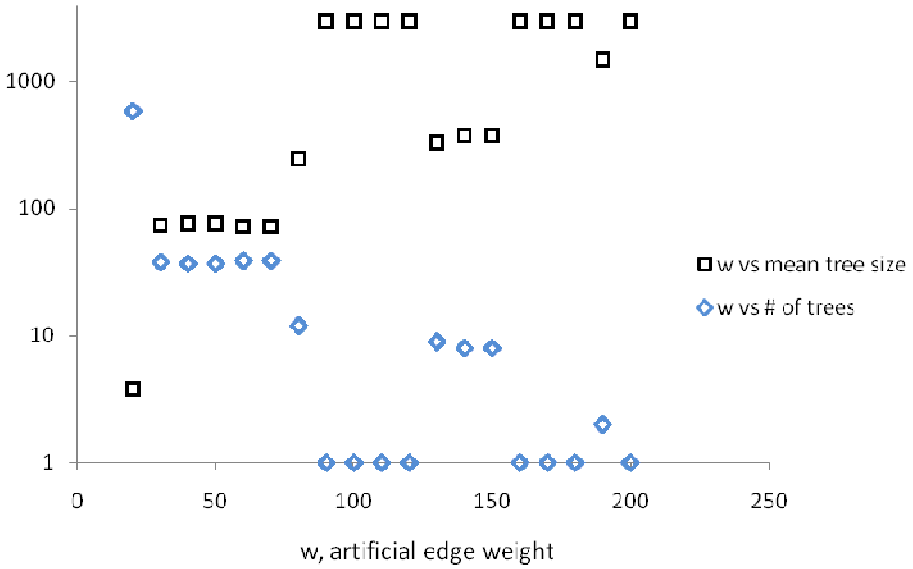

Figure S2 Effect of the weight of edges to the artificial root node (ω) on mean tree sizes and the number of trees in the resulting forest for several β values for **(a)** the first random set (3,000 nodes and 7,500 edges) and **(b)** the second random set (of 3,000 nodes and 15,000 edges).

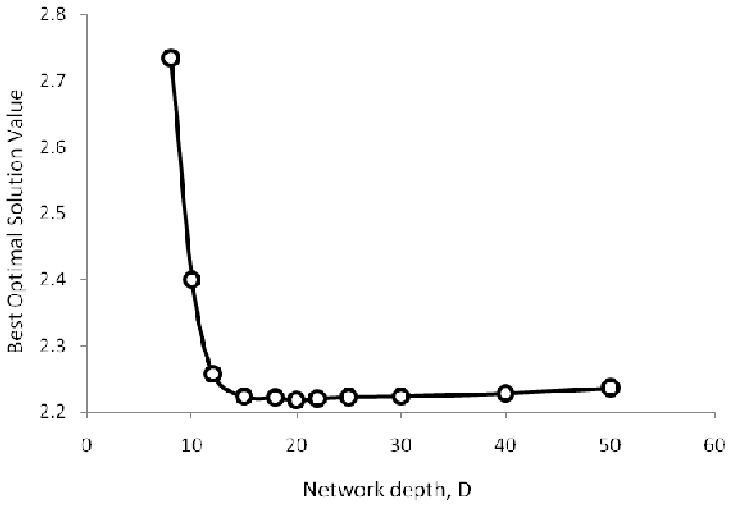

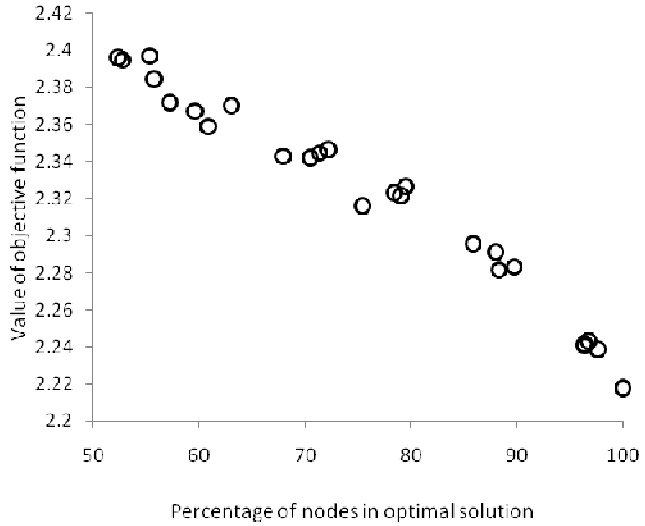

Figure S3 (a) The effect of maximum network depth (D) on the best optimal solution value. The minimum value is achieved when depth equal to 20. (b) Overlap of the sub-optimal solutions. These suboptimal solutions are obtained by adding uniform noise to the edge weights. With the increasing noise the percentage of nodes in optimal solution decreases and value of the objective function increases.

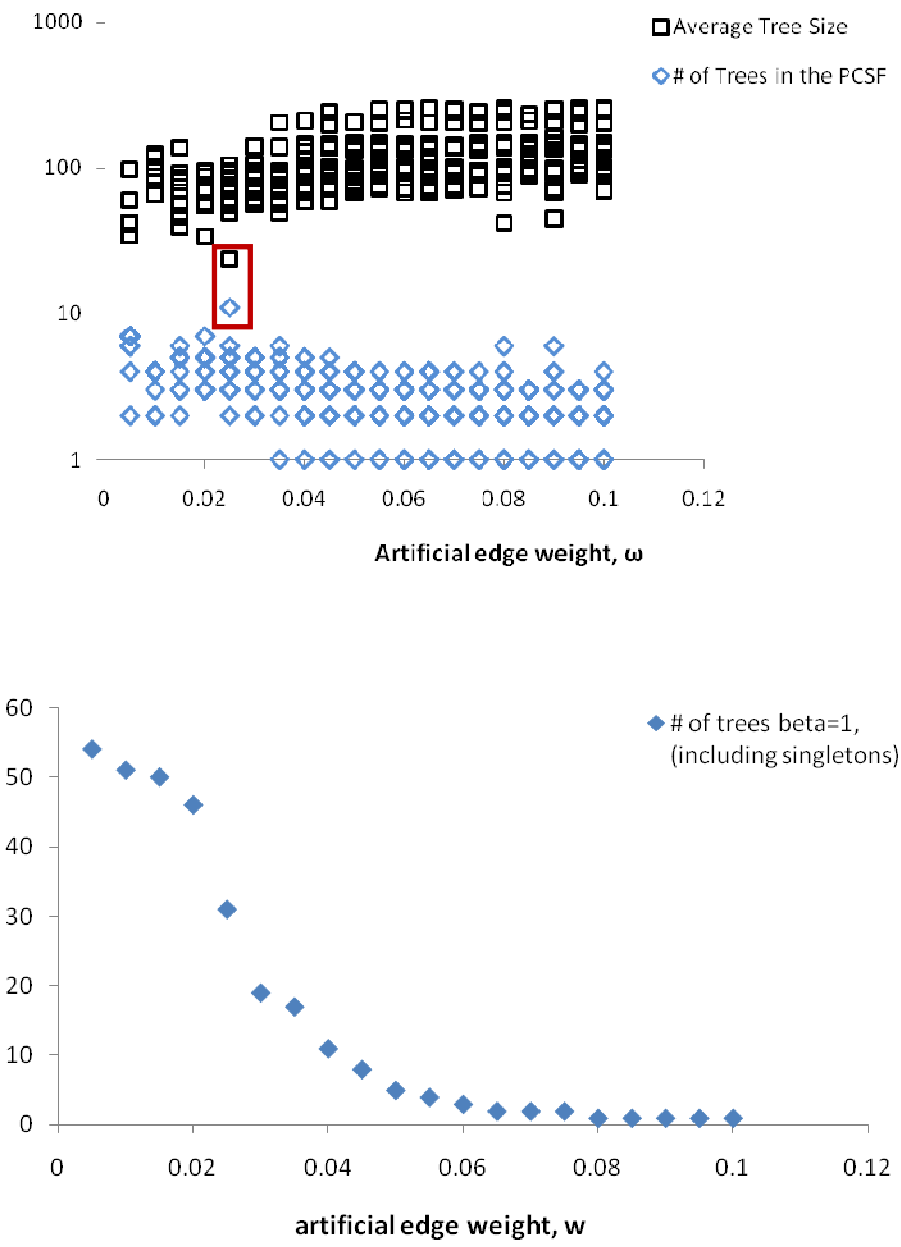

Figure S4 Effect of the weight of edges to the artificial root node (ω) on mean tree sizes and the number of trees in the resulting forest for the yeast pheromone response data. (A) Mean tree sizes and number of trees in the resulting forests as the artificial edge weight, ω, is varied for β values within the interval [1,20] (singletons are excluded). (B) The number of sub-trees in the PCSF as the artificial edge weight, ω, is varied (singletons are included) for one β value.

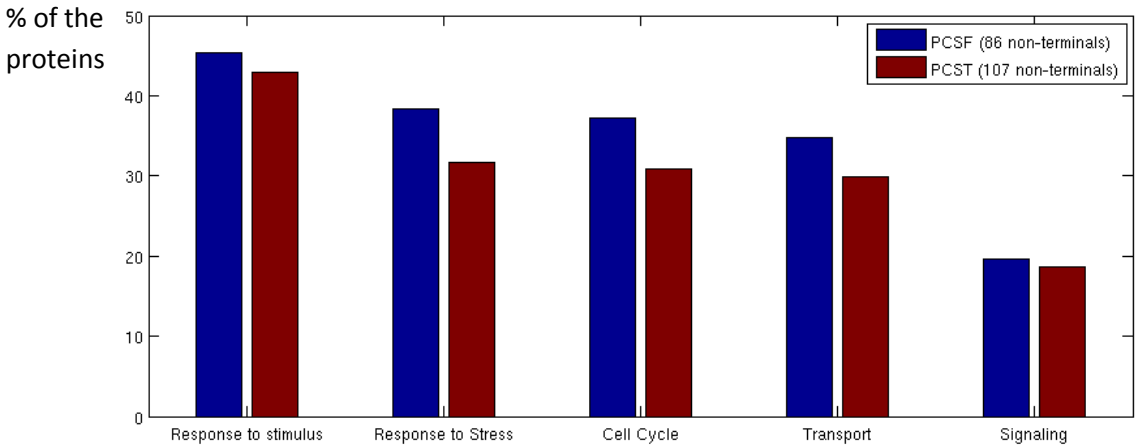

Figure S5 Functional enrichment of the non-terminal proteins in yeast PCST and PCSF.

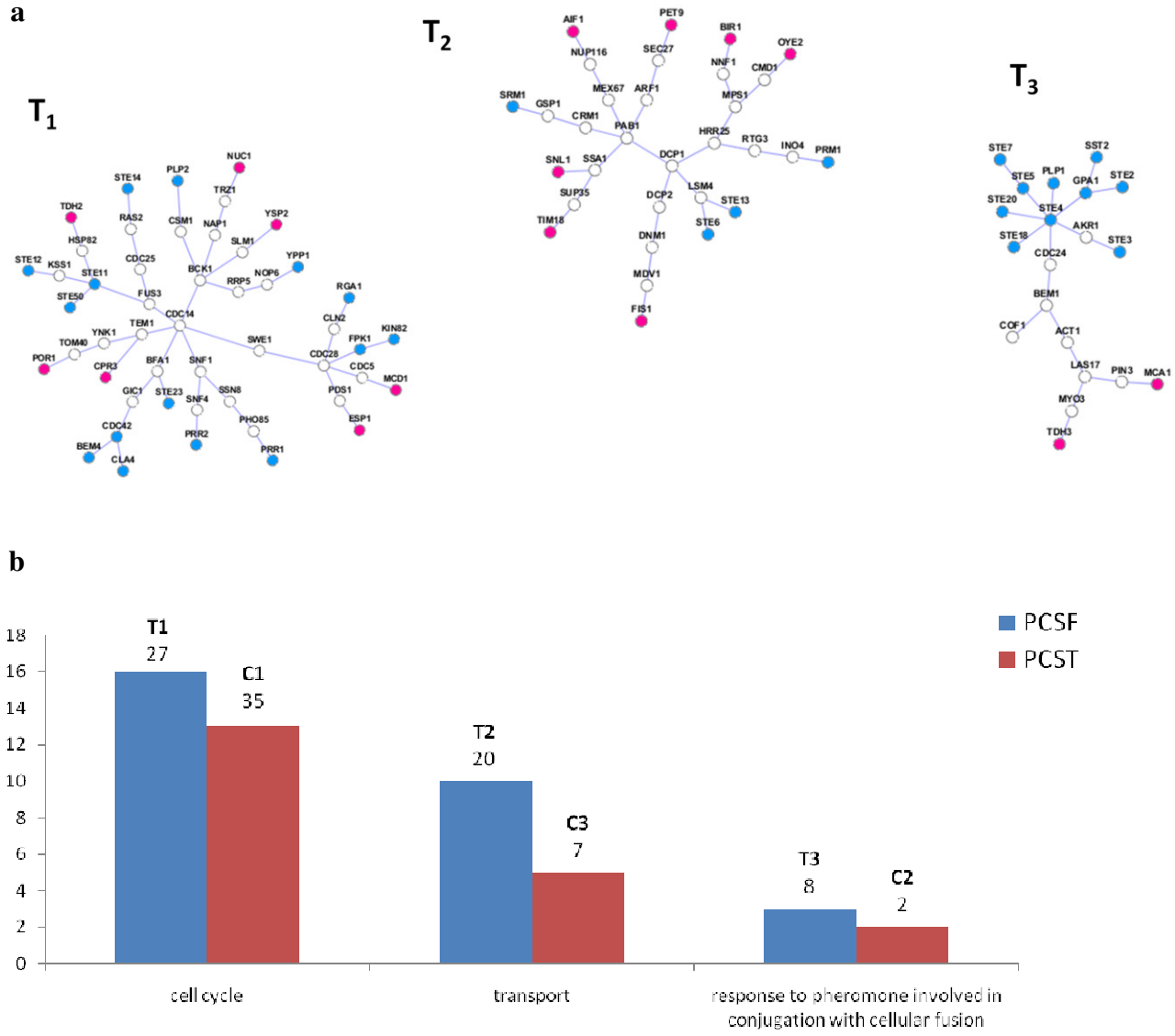

Figure S6 (a) The PCSF of the yeast interactome where the terminal nodes are the part of either the pheromone response or apoptosis processes. In the resulting forest, there are three sub-trees. Here, red colored nodes are terminals in apoptosis pathway while blue colored nodes are terminal nodes in pheromone response. T1 is enriched in in response to pheromone (p-value=4.13×10^{-18}), regulation of cell cycle (p-value=5.71×10^{-10}) and signal transduction (p-value=4.97×10^{-10}); T2 is enriched in apoptosis and biogenesis (p-value= 1.93×10^{-9}) and T3 is enriched in reproduction (p-value=9.11×10^{-13}), cell budding (9.83×10^{-4}), actin cytoskeleton organization (p-value=1.49×10^{-4}) and in response to pheromone (3.43×10^{-17}). **(b)** Comparison of non-terminal nodes in the sub-trees in PCSF and in the clusters in PCST.

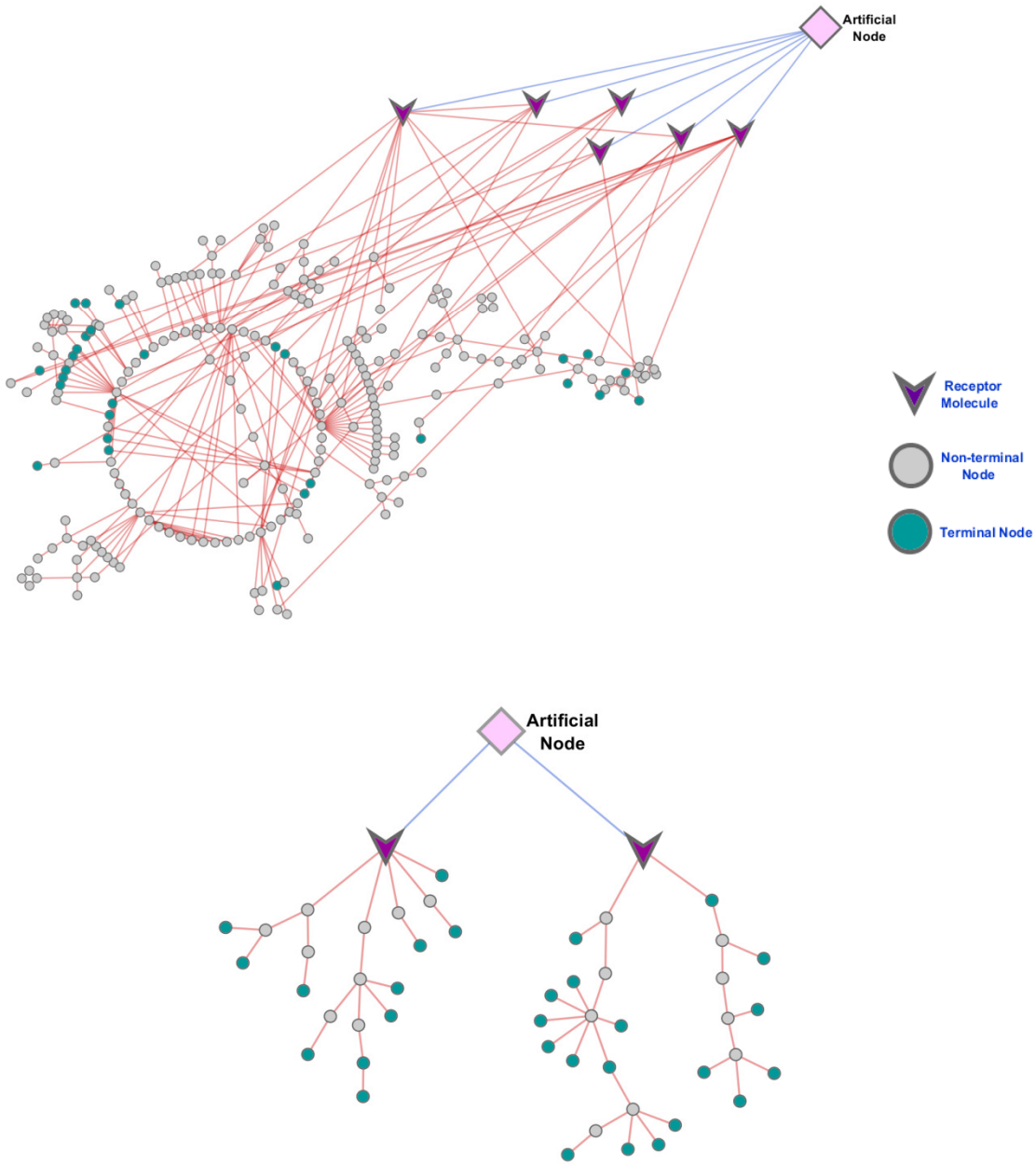

Figure S7 Schematic for identifying signaling from receptors. **(a)** An artificial node is connected only to cell-surface receptors. In the second layer, receptor molecules are connected to all other proteins through the interactome. **(b)** After constructing the prize-collecting Steiner tree and removing the artificial node, the resulting PCSF contains two sub-trees where each sub-tree has one receptor as the root node.

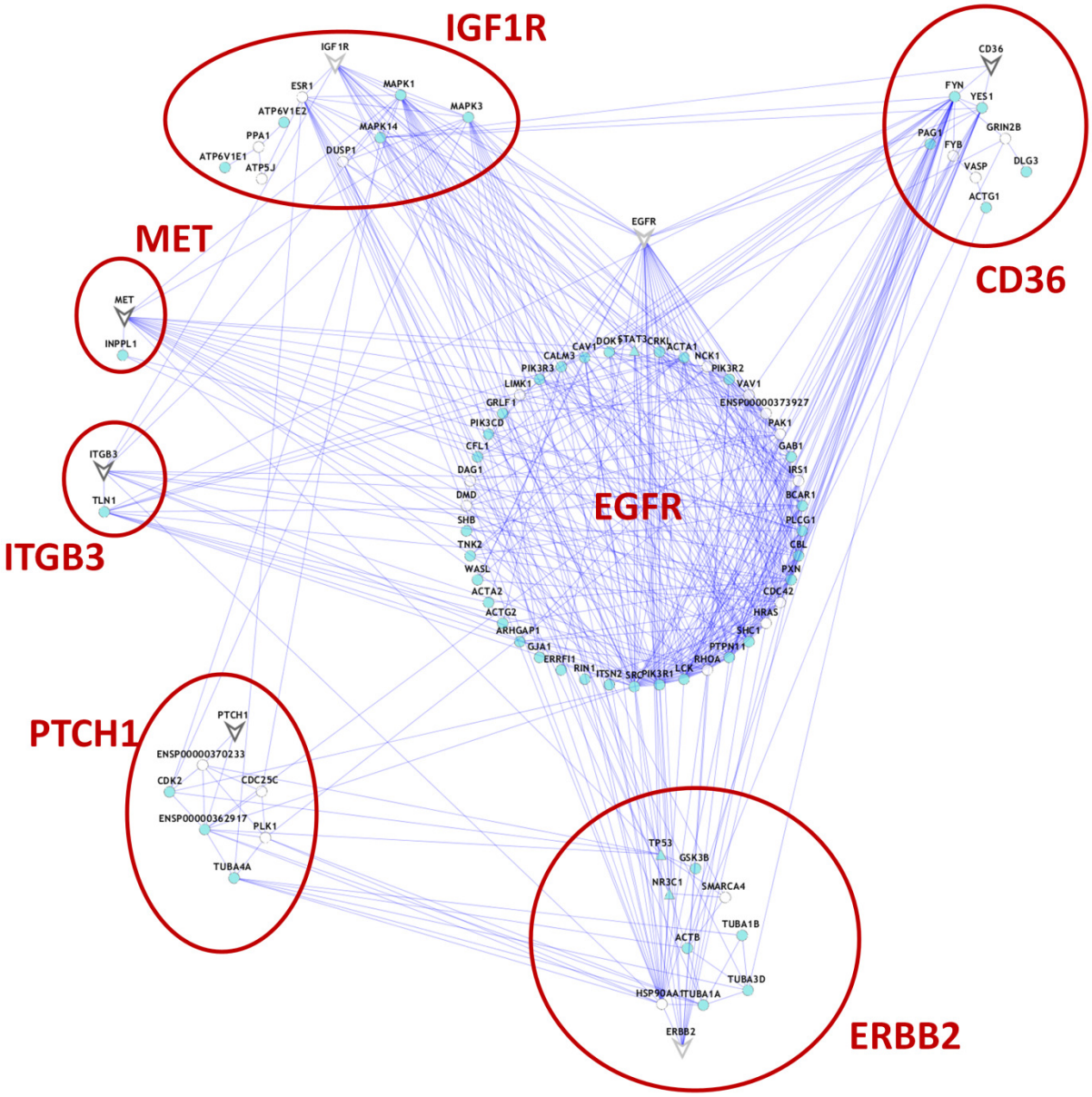

Figure S8 The PCSF obtained for GBM is augmented by the edges in the original interactome.

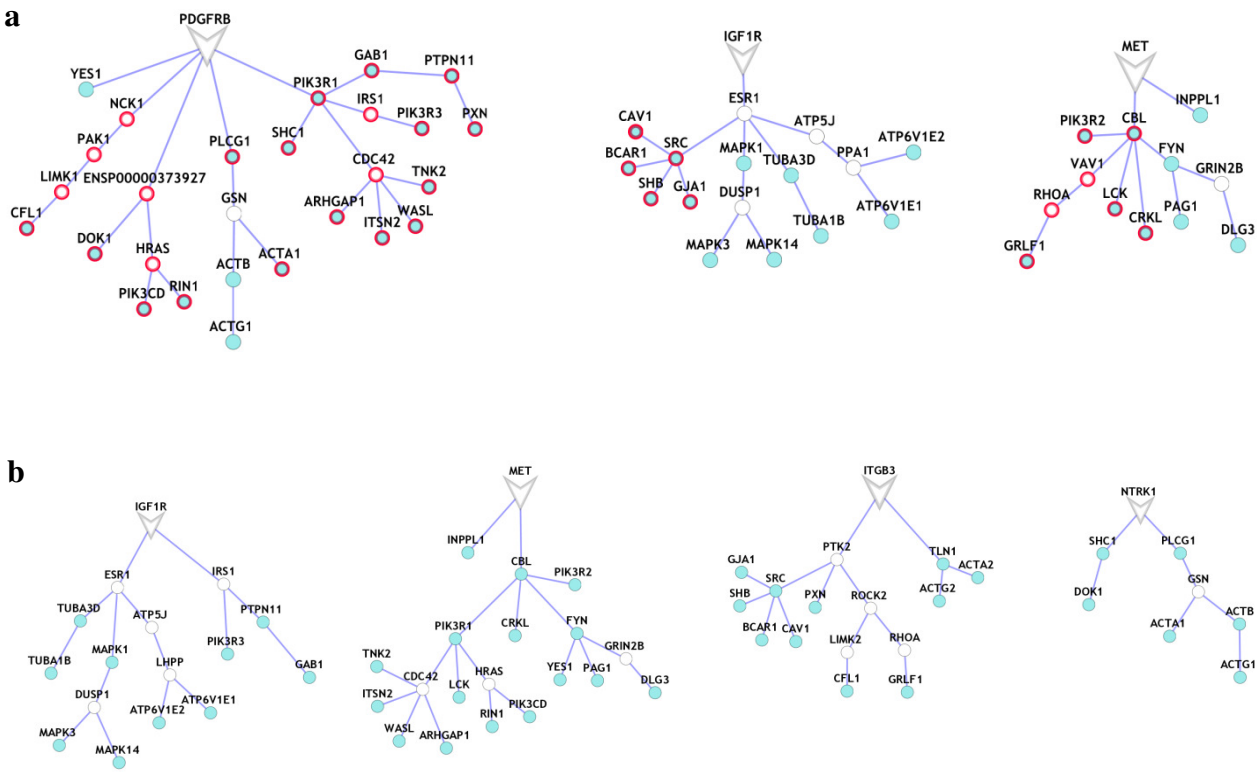

Figure S9 Solution forests after in silico knockout experiments. **(a)** Forest obtained after removing EGFR and ERBB2. Nodes that are downstream of EGFR in the original network are outlined in red. **(b)** Forest obtained after removing EGFR, ERBB2 and PDGFR.